Maerz, N. H., and Zhou, W., 2000. **Calibration of optical digital fragmentation measuring systems.** FRAGBLAST, The International Journal For Blasting and Fragmentation, v 4, no.2, pp. 126-138.

Calibration of optical digital fragmentation measuring systems

Norbert H. Maerz,
Rock Mechanics and Explosives Research Center, University of Missouri-Rolla

Wei Zhou,
Department of Geological Engineering, University of Missouri-Rolla

ABSTRACT: Optical granulometry systems like WipFrag are required to measure fragments in situ. That is to say, the fragments are in piles where sorting takes place, where fragments are partially overlapped, and where fines may not be seen because they fall in and behind the coarser fragments, or where the fines are simply too small to be seen. As a result, optical systems tend typically to overestimate the size of the distribution, and underestimate the variability of the distribution. The wider the size distribution being measured, the more severe the problem is. This paper presents the results of a study that suggests that these systematic errors can be significantly reduced by calibration.

1 INTRODUCTION

Optical digital imaging systems such as WipFrag, (Maerz et al., 1996) are increasingly being used to characterize fragmentation in the mining, comminution and materials handling industries (Franklin et al, 1996). Gradation measurements can be completely automated, eliminating the subjectivity of manual measurements. Because of extremely low per unit costs, many more measurements can be made, resulting in lower sampling errors (Maerz, 1996a, Palangio and Franklin, 1996). Interruption of production processes is not required, and results are available in a very short time, allowing timely adjustments to production methods. In the case of large blocks or large volumes of rock, screening is just too prohibitive, and optical methods are the only alternative.

At the same time, optical methods have associated errors and inaccuracies. Some of the errors, such as block miss-identification as a result of poor images, poor lighting, and perspective errors, can be remedied by improving the quality of the imaging. Sampling errors can be decreased by systematic sampling strategies, and by analyzing a larger number of samples. Some errors, such as those caused by the imaging of multi-colored rock and rock types with heavily textured surfaces, may be difficult to deal with. By far the greatest error in optical systems is a result of the consequence of "hidden fines" (Maerz and Zhou, 1999).

These types of errors can be rectified in a number of ways. Calibration is the most popular solution, and has been the subject of recent publications (Barkley and Russell, 1999; Katsabanis, 1999).

2 THE HIDDEN FINES PROBLEM

Optical granulometry systems like WipFrag are required to measure fragments in situ. That is to say, the fragments are in piles where sorting takes place, where fragments are partially overlapped, and where fines may not be seen because they fall in and behind the coarser fragments, or they are simply too small to be seen.

The hidden fines error in optical systems stems from the fact that, in an image of an assemblage of rock fragments, the small pieces, especially in the case of a wide or well-graded distribution, are typically hidden from view in the image. In a narrow, or well-sorted distribution, this tends not to be a problem (Maerz, 1998). The error occurs because of one of two reasons:

1. The smaller particles are too small to resolve or resolve effectively, because of the limitation in the range of sizes that can be viewed and identified on a single image, or

2. The smaller particles are hidden from view having fallen in and behind the larger particles.

The hidden fines error results typically in an over-estimation of the mean size of the distribution, and in an under-estimation of the variability of the distribution. The more well graded the distribution being measured, the more severe the problem is. Experience measuring fragmentation has shown however, that this error is systematic.

3 HIDDEN FINES SOLUTIONS

In the WipFrag system, there are three methods available for making corrections for missing fines. There is 1) an analytical correction that is built into the system, 2) images obtained at different scales of observation can be merged, and 3) Rosin-Rammler empirical calibrations can be used.

In some cases it is not necessary to apply these kinds of corrections. This is true for uniformly distributed assemblages. Where only direct comparisons are to be done, and only relative sizes are important, it may also not be necessary to apply fines corrections (Maerz et. al., 1987).

3.1 Analytical Correction

The WipFrag System, as a basis for reconstructing three-dimensional distributions from two-dimensional measurements, uses principles of stereology and geometric probability to reconstruct or unfold the distribution (Maerz, 1996b). Part of that unfolding process compensates for missing fines by considering the smaller probability of a finer fragment being detected in a sampling plane.

The effectiveness of this correction is however, limited to moderately well graded distributions. The studies described in this paper suggest that this correction is most effective at a Rosin-Rammler *n*-value of about 2.5.

3.2 Zoom-Merge Correction

Because the analysis of single images is inherently limited to resolving less than two orders of magnitude of fragment linear size, the ability to measure fines can be improved by doing a merged analysis of images that have been acquired at different scales of observation (Santamarina et. al., 1996). This involves acquiring numerous "zoomed" images, and merging them in the final analysis.

Although this method has the potential of producing extremely reliable results, it is however cumbersome because of the need to take multiple images while managing the different combinations of camera zoom and panning, and tracking the different images to the final analysis stage.

3.3 Rosin-Rammler Empirical Calibration Correction

The most effective way to include the correct weight of fines in the analysis is to do an empirical calibration. In this process we make the assumption that for a given process, such as blasting, grinding or crushing, the shape (or slope) of the distribution is more or less constant. Consequently, changes in the process will tend to result in shifts in the distribution, i.e., changes in central tendency rather than variability.

If this assumption is correct, then although we cannot measure the changes at the fine end of some distributions, studies have shown that we can however, predict the changes at the fine end of the distribution with the measured differences in the coarse end of the distribution (Simkus and Dance, 1998). Consequently, these changes can, with a reasonable degree of accuracy, be predicted by a constant calibration factor.

WipFrag handles this calibration by fitting a Rosin-Rammler Curve to the measured data. While arguments and discussion rage as to the appropriateness of this distribution, it is as good as any other; and it is easy to work with because it is a two-parameter distribution, with one parameter representing central tendency (x_c), and the second the slope or variability of the distribution (n).

The Rosin-Rammler equation is:

$$y = 1 - \exp\left[-\left(\frac{x}{x_c} \right)^n \right] \tag{1}$$

Where: y is the cumulative percent passing,
x is the particle size,
x_c is the characteristic size of the distribution (63.2% passing),
n is a parameter describing the size range of the distribution,

The calibration factors are then added to the equation:

.

$$y = 1 - \exp\left[-\left(\frac{x}{x_c \times x_{ca}} \right)^{n \times n_a} \right] \quad (2)$$

Where: x_c is the characteristic size, as measured by WipFrag,
n as measured by WipFrag ,
x_{ca}, is the adjustment relating the true characteristic size (x_c) to the WipFrag measured size,
n_a, is the adjustment relating the true n-value to the WipFrag measured n-value.

Calibration Correction Using Screening

The x_{ca} and n_a calibration parameters can be determined by screening a test sample of rock while simultaneously analyzing it using image analysis. A test sample of suitable quantity is identified on a belt, pile, or anywhere else, in the exact position and state of mixing/segregation that the measurement required for production would be. Multiple images of the assemblage are taken, at an appropriate scale of observation, and the images analyzed and merged. Then, the assemblage is screened. The results of the screening analysis and image analysis are compared, and from that comparison, calibration factors can be determined.

Calibration Using Model Studies

The use of scaled-down crushed rock samples for preparing calibrations is appealing, because it does not require the manipulation and handling of tons of rock, and extraordinary screening methods.

The rationale behind using scaled down samples within the context of a single image, is that the absolute size of the particles are irrelevant to the analysis, save for the value of the scaling factor. The relevant factors are two variables:

1. The size of the particles relative to the image, and,
2. The slope of the size distribution.

If the first variable is held constant throughout the analysis, and the slope of the distribution is varied then a calibration can be specified as a function of the slope of the distribution.

To this end, seven manufactured distributions of crushed limestone rock samples were generated using conventional sieving, with Rosin-Rammler n-values (slope) of 0.5, 0.75, 1.0, 1.25, 1.5, 2.0, and 3.0 (Figure 1). The samples consisted of four kilograms of rock each with a maximum size of 25.4 mm. Figure 2 shows the results of the calibration tests, for the samples in Appendix 1. The first variable (relative size) was held constant by acquiring an image in which the length of largest common block in the image was approximately 1/10 of the width of the image. Each distribution was analyzed using WipFrag with great care taken to set the edge detection variables. No manual editing was done. The calibrations were then back-calculated.

The calibration results in Figure 2 show that the calibration is both consistent and predictable. Specifically, the results indicate that:

1. It is possible to get accurate values of central tendency for distributions with Rosin-Rammler n-values in the range of 1.0 to 3.0 even *without calibration*.

2. Significant overestimation of the characteristic size occurs when the distribution has a true *n*-value of 0.75, because of the inability of the system to resolve the relatively numerous fines. Distributions with lower *n*-values may be difficult to analyze.

3. The n_a factor is a linear function of the true *n*-value of the distribution.

4. At a true *n*-value of about 2.5 the measurement results should be very accurate for both *n* and x_c *without calibration*.

The standard calibration factors should apply to most rock types and situation, assuming the same precautions described above are used. The only thing required is an estimate of the true *n*-value.

Visual Estimation of n-value for Selecting Calibration Factors
One way to select the appropriate calibration factors is to estimate visually the Rosin-Rammler *n*-value. Cunningham's compaphoto technique for assessing rock pile fragmentation from photographs of standardized muck piles, although not viable for that purpose, was judged to have worked well in terms of identifying uniformity index (*n*-values) (Cunningham, 1996).

To decide which of these calibrations to use requires a visual estimate of the true *n*-value. This is done by comparing the type pictures and descriptions of Figure 3, with the actual distribution being measured.

For full-scale blasts, results of screening indicate that *n*-values are between 0.75 and 1.75 (Ryan, 1998).

Calculating n-values for Selecting Calibration Factors
Cunningham (1987) suggests that the Rosin-Rammler *n*-value (uniformity index) can be calculated by the following approximation:

$$n = \left(2.2 - 14\left[\frac{B}{d}\right]\right) \times \left(\frac{1+\frac{S}{B}}{2}\right)^{0.5} \times \left(1 - \frac{D}{B}\right) \times \left(\frac{abs[l_c - l_b]}{l_{cl}} + 0.1\right)^{0.1} \times \left(\frac{L_t}{H_b}\right) \qquad (3)$$

Where:

B is the burden [m]
d is the hole diameter [m]
S is the spacing [m]
D is the drill hole deviation [m/m]
l_c is the column charge length [m]
l_b is the bottom charge length [m]
l_{cl} is the total charge length (l_c + lb) [m]
H_b is the bench height [m]

Although this does not consider geological factors, which clearly influence the distribution of fragmentation, it may still be a useful estimate

Proposed Automatic Selection of Calibration Factors
Figure 2 shows that the error in calculating the *n*-value using WipFrag is both systematic and predictable. There is a linear relationship between the two. This relationship may be able to be exploited by using the relationship between the measured *n*-value and the empirically derived *n*-value error (Figure 3) to get the "true" *n*-value. The true *n*-values would then in turn used to automatically select calibration factors as described by Figure 2.

Figures 4 and 5 show the results of applying the automatic calibration to the test samples. These show that both raw (measured before calibration) and auto-calibrated results are more accurate for x_c than for *n*. Figure 5 shows that the scattering which is a function of sampling bias during the imaging process, even under these controlled conditions, creates errors, which are not corrected by the auto-calibration process. If the calibrations are not selected automatically, i.e., they are selected accurately by visual inspection, the errors are less pronounced. Thus it is not clear at this time whether auto calibration is a useful option.

4 CONCLUSIONS

1. Optical imaging systems have associated errors with resolving fines. This is true especially with well-graded distributions, where the optical systems tend to overestimate the central tendency of the distribution and underestimate the variability. These errors are systematic.

2. When imaging systems are used for the purposes of comparison, e.g. over time, between two blast designs, etc., the uncorrected imaging results may be used, ignoring the hidden fines problem.

3. Because the errors are systematic, empirical calibrations can be used to successfully correct for hidden fines. This requires either a size/situation specific calibration to screening result, or the use of a generic calibration model presented here. Using that model requires careful scaling and processing of images, and an estimate of true Rosin-Rammler *n*-value.

4. The Rosin-Rammler *n*-value may also be determined automatically by using a calibration that relates the measured *n*-value to the true *n*-value.

5 REFERENCES

Barkley, T. and Russell, C. 1999. Evaluation of optical sizing methods. *Proceedings of the 25th Annual Conference on Explosives and Blasting Technique, Nashville, Tennessee, USA*, Vol. II, pp. 305-323.

Cunningham, C. 1987. Fragmentation estimations and the Kuz-Ram model - four years on. *Proceedings of the 2nd International Symposium on Rock Fragmentation, Keystone, Colorado,* pp. 475-487.

Cunningham, C. 1996. Lessons form the Compaphoto technique of fragmentation measurement. *Proceedings of the FRAGBLAST 5 Workshop on Measurement of Blast Fragmentation, Montreal, Quebec, Canada*. Franklin, J. A, and Katsabanis, T., (ed.). A. A. Balkema, pp. 53-57.

Franklin, J. A., Kemeny, J. M. and Girdner, K. K. 1996. Evolution of measuring systems: A review. *Proceedings of the FRAGBLAST 5 Workshop on Measurement of Blast Fragmentation, Montreal, Quebec, Canada*. Franklin, J. A, and Katsabanis, T., (ed.). A. A. Balkema, pp. 47-52.

Katsabanis, P. D. 1999. Comparison between laboratory analysis and sieving using laboratory scale model muckpiles. *Proceedings of the 25th Annual Conference on Explosives and Blasting Technique, Nashville, Tennessee, USA,* Vol. II, pp. 323-332.

Maerz, N. H. 1996a. Image sampling techniques and requirements for automated image analysis of rock fragmentation, 1996**.** *Proceedings of the FRAGBLAST 5 Workshop on Measurement of Blast Fragmentation, Montreal, Quebec, Canada*. Franklin, J. A, and Katsabanis, T., (ed.). A. A. Balkema, pp. 115-120.

Maerz, N. H. 1996b. Reconstructing 3-D block size distributions from 2-D measurements on sections**.** *Proceedings of the FRAGBLAST 5 Workshop on Measurement of Blast Fragmentation, Montreal, Quebec, Canada*. Franklin, J. A, and Katsabanis, T., (ed.). A. A. Balkema, pp. 39-43.

Maerz, N. H. 1998. Aggregate sizing and shape determination using digital image processing. *Center For Aggregates Research (ICAR) Sixth Annual Symposium Proceedings*, pp. 195-203.

Maerz, N. H., Franklin, J. A. and Coursen, D. L. 1987. Fragmentation measurement for experimental blasting in Virginia. *S.E.E., Proc. 3rd. Mini-Symposium on Explosives and Blasting Research,* pp. 56-70.

Maerz, N. H., Palangio, T. C. and Franklin, J. A. 1996. WipFrag image based granulometry system. *Proceedings of the FRAGBLAST 5 Workshop on Measurement of Blast Fragmentation, Montreal, Quebec, Canada*. Franklin, J. A, and Katsabanis, T., (ed.). A. A. Balkema, pp. 91-99.

Maerz, N. H. and Zhou, W. 1999. Optical digital fragmentation measuring systems - inherent sources of error. *Accepted for publication, FRAGBLAST- The International Journal For Blasting and Fragmentation*.

Palangio, T. C. and Franklin, J. A., 1996. Practical guidelines for lighting and photography. *Proceedings of the FRAGBLAST 5 Workshop on Measurement of Blast Fragmentation, Montreal, Quebec, Canada*. Franklin, J. A, and Katsabanis, T., (ed.). A. A. Balkema, pp. 111-114.

Ryan, J. 1998. Compromising Technology with Field Experience in Fragmentation Evaluation. *State-of-the-Art, Blasting Technology Instrumentation and Explosives Applications, Eighth High-Tech Seminar,* pp. 255-268.

Santamarina, J. C., Morely, M., Franklin, J. A. and Wang, D. S. 1996. Development and testing of a zooming technique for fragmentation measurement**.** *Proceedings of the FRAGBLAST 5 Workshop on Measurement of Blast Fragmentation, Montreal, Quebec, Canada*. Franklin, J. A, and Katsabanis, T., (ed.). A. A. Balkema, pp. 133-139.

Simkus R. and Dance A., 1998. Tracking hardness and size: Measuring and monitoring ROM ore properties at Highland Valley Copper. *Proceedings Mine to Mill 1998 Conference*. Australasian Institute of Mining and Metallurgy: Melbourne, pp. 113 -119.

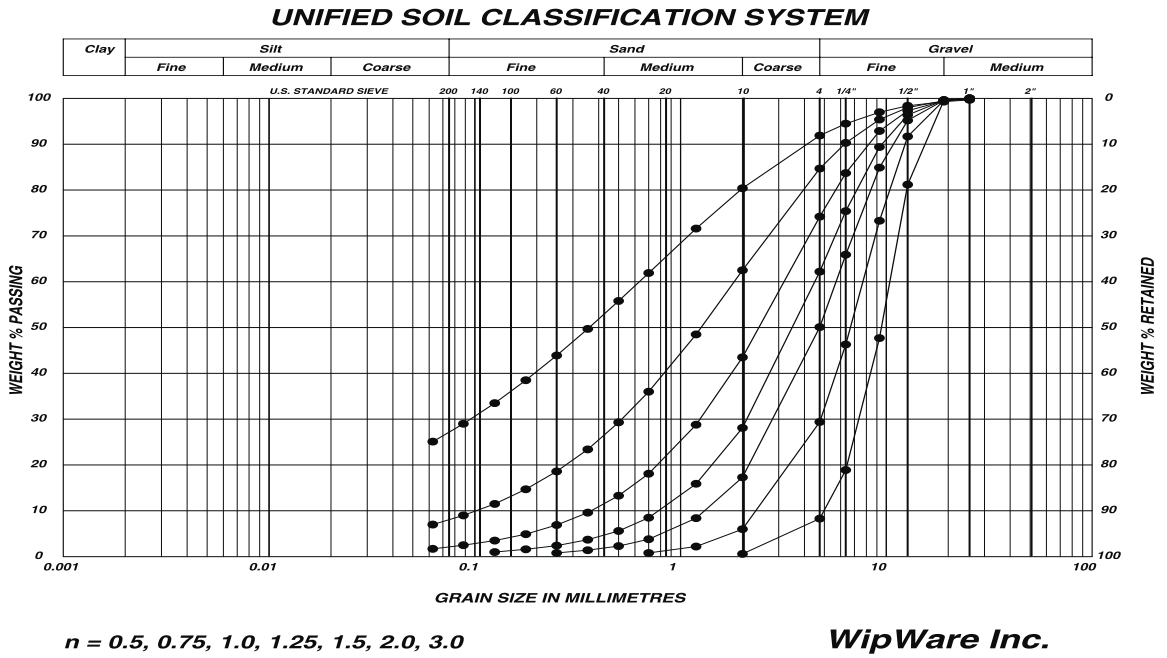

Figure 1. Gradations of the fabricated crushed rock samples

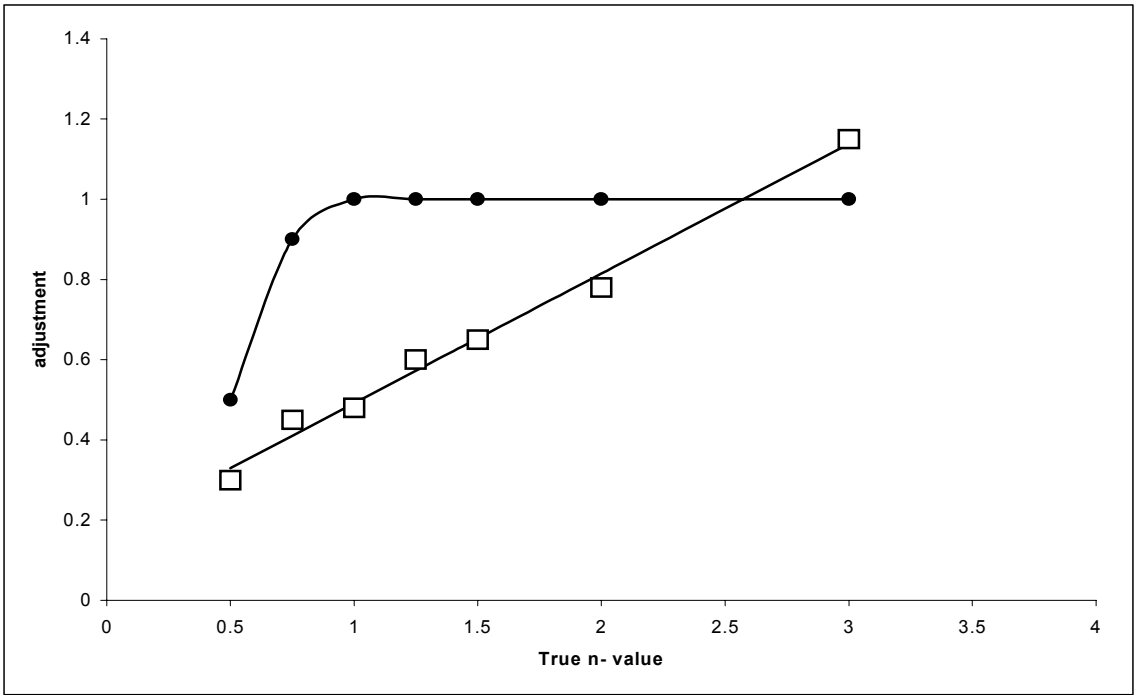

Figure 2. x_c and n calibration Factors. Filled circles are the x_{ca} adjustment factors (1 = no adjustment), and the squares are the n_a adjustment factors.

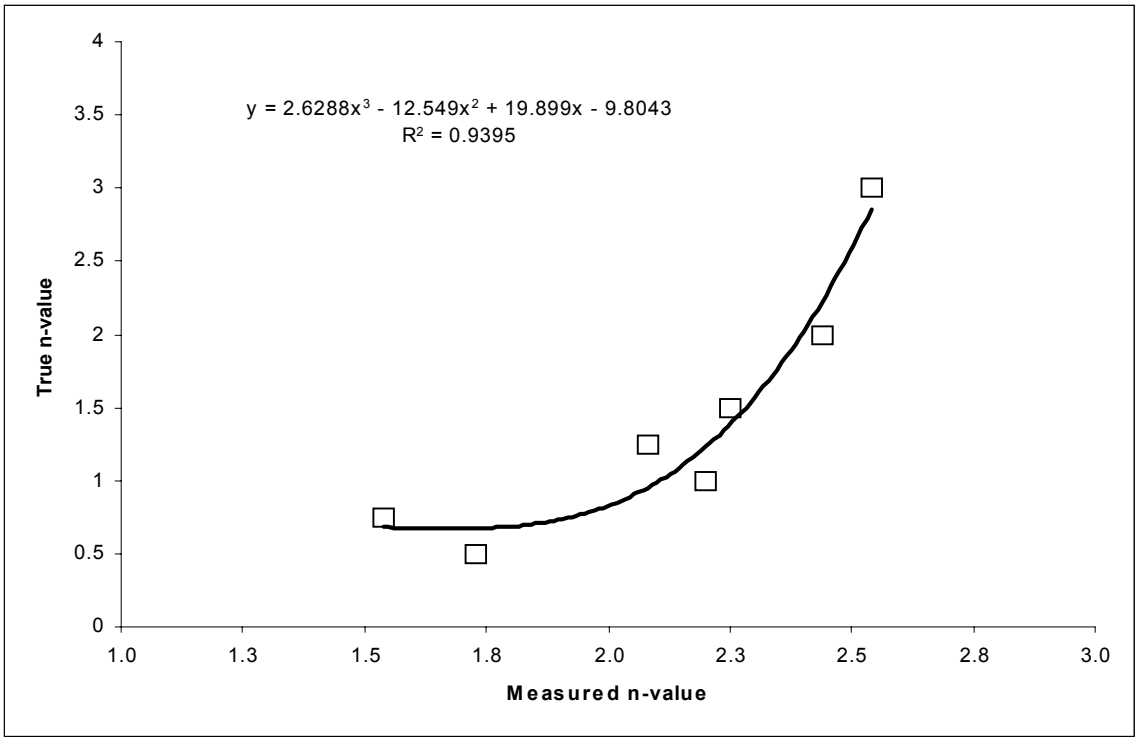

Figure 3. n-value error calibration fitted with a third-order polynomial. Scatter is a function of sampling bias during the imaging stage.

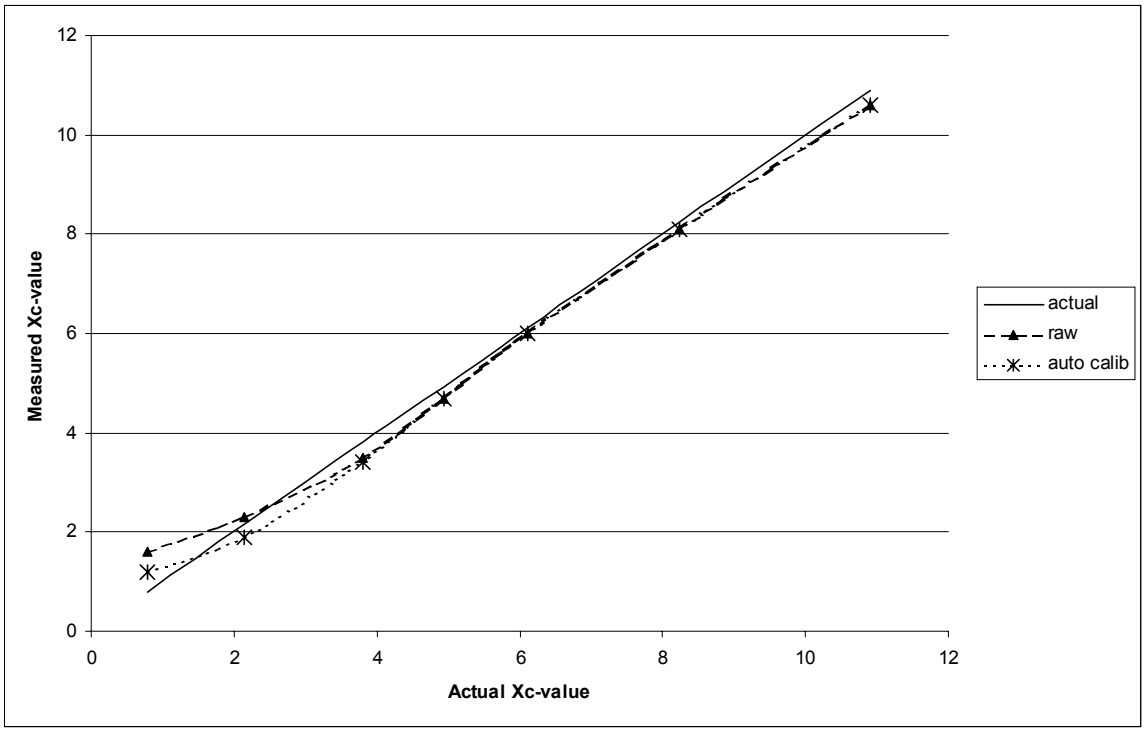

Figure 4. Relationship between actual x_c-values, raw x_c values, and auto-calibrated x_c-values.

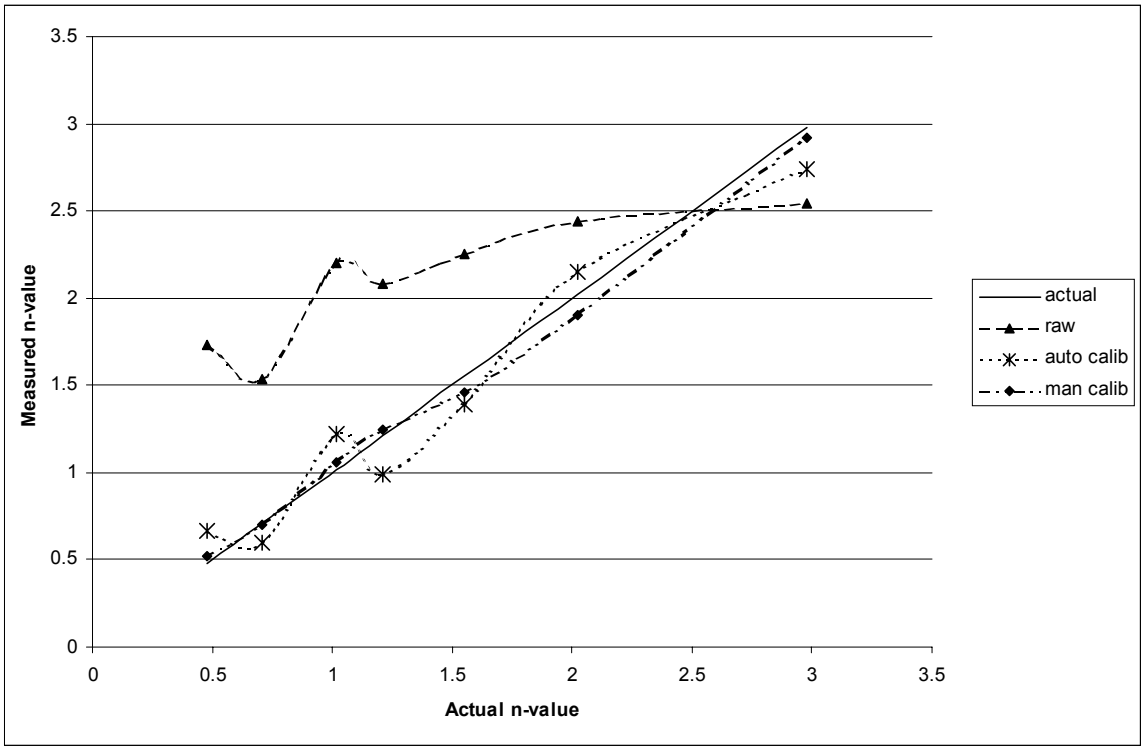

Figure 5. Relationship between actual *n*-values, raw *n*-values, manually selected calibration, and auto-calibrated *n*-values. The variability in the raw and auto-calibrated curves is a function of sampling bias during the imaging stage.

APPENDIX 1: IMAGES OF THE "TYPE" DISTRIBUTIONS

n=3.0. Characterized by a very uniform size distribution, where the smallest common visible block is about 1/3 the size of the largest common block. (The white scale bar represents 1 inch.)

n=2.0. Characterized by a fairly uniform size distribution, where the smallest common visible block is about 1/5 the size of the largest common block. The ratio of the number of largest common blocks to smallest common blocks is about 20:1. (The white scale bar represents 1 inch.)

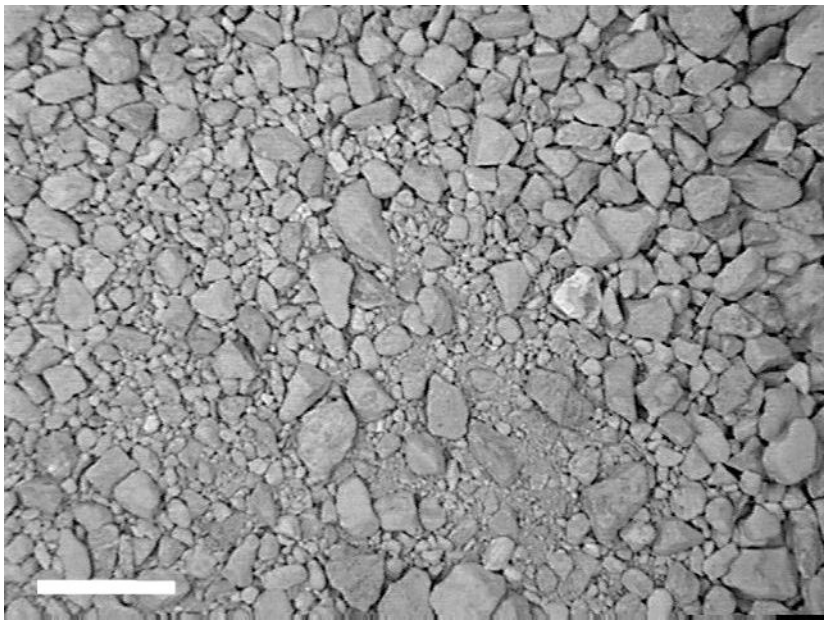

n=1.5. Characterized by a moderately uniform size distribution, where the smallest visible common block is about 1/8 the size of the largest common block. The ratio of the number of the largest common blocks to smallest common blocks is about 8:1. Small areas of particles that are too small to be resolved cover about 5% of the image. (The white scale bar represents 1 inch.).

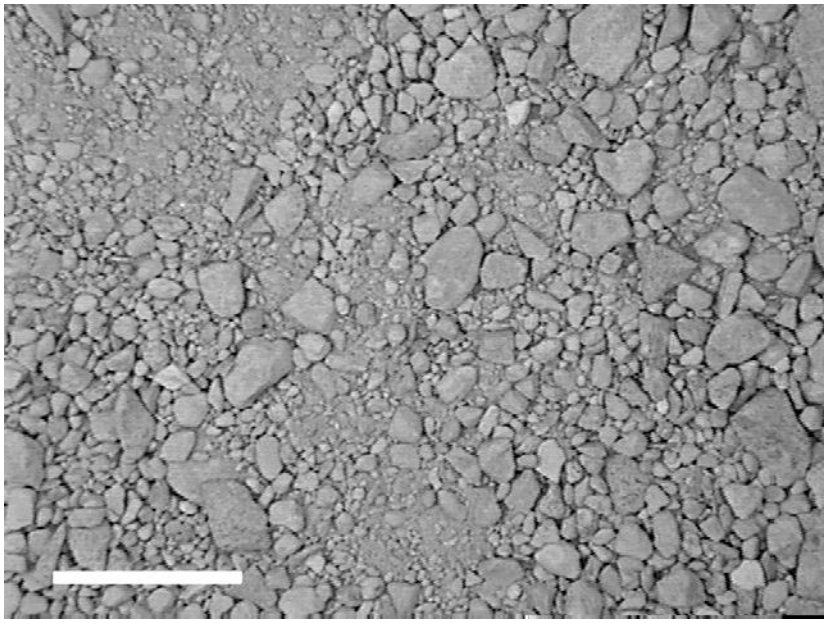

n=1.25. Characterized by a poorly uniform size distribution, where the smallest common visible block is about 1/12 the size of the largest common block. The ratio of the number of largest common blocks to smallest common blocks is about 2:1. Areas of particles that are too small to be resolved cover about 15% of the image. (The white scale bar represents 1 inch.).

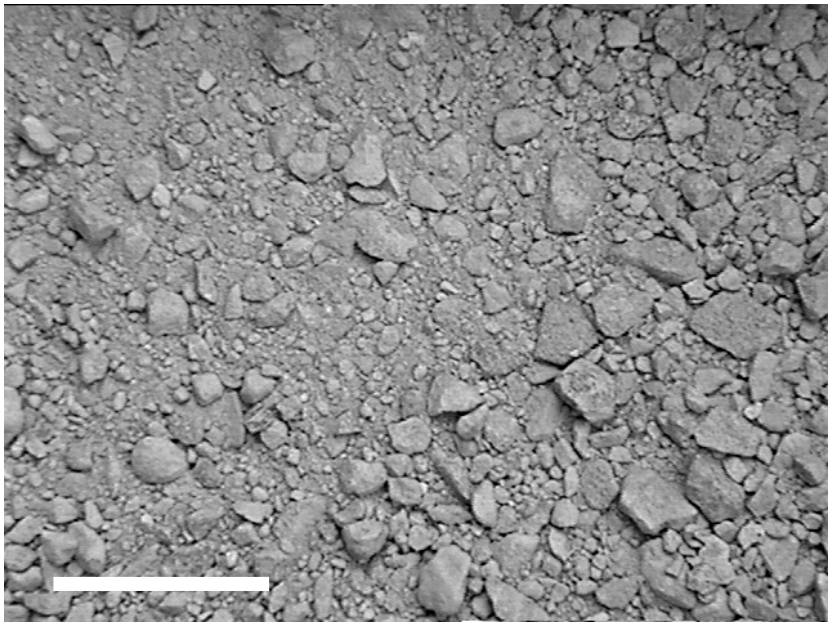

n=1.0. Characterized by a moderately well graded size distribution, where the smallest common visible block is about 1/16 the size of the largest common block. The ratio of the number of largest common blocks to smallest common blocks is about 1:2. Areas of particles that are too small to be resolved cover about 30% of the image. (The white scale bar represents 1 inch.).

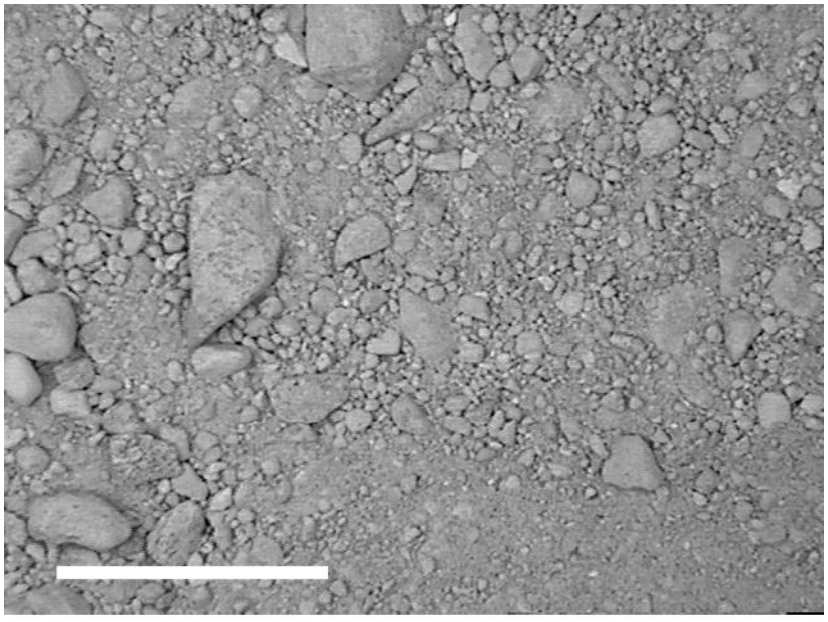

n=0.75. Characterized by a well-graded size distribution, where the smallest common visible block is about 1/20 the size of the largest common block. The ratio of largest common blocks to smallest common blocks is about 1:8. Areas of particles that are too small to be resolved cover about 50% of the image. (The white scale bar represents 1 inch.).

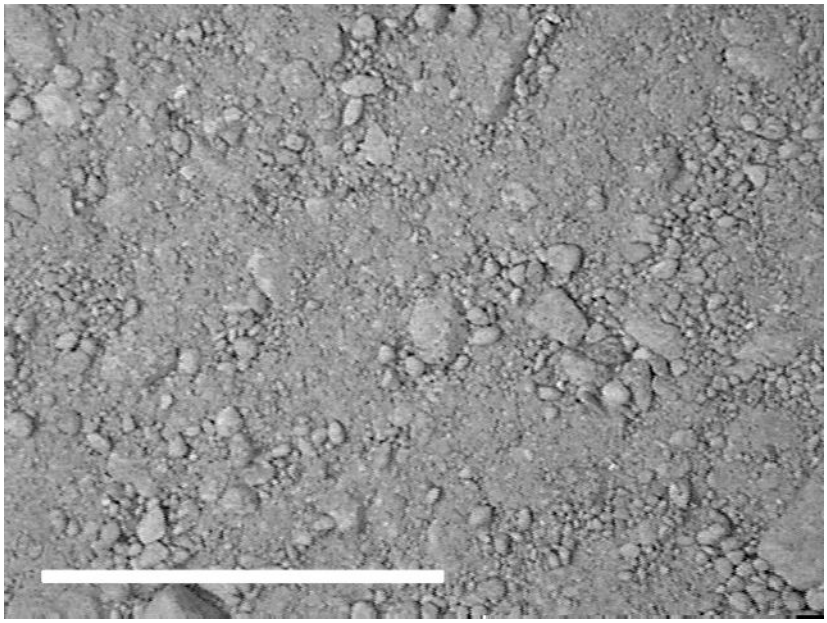

n=0.5. Characterized by a very well graded size distribution, where the smallest common visible block is about 1/20 the size of the largest common block. The ratio of largest common blocks to smallest common visible blocks is about 1:15. Areas of particles that are too small to be resolved cover over 50% of the image. (The white scale bar represents 1 inch.).